Acta Biomaterialia xxx (xxxx) xxx

Contents lists available at ScienceDirect

Acta Biomaterialia

journal homepage: www.elsevier.com/locate/actbio

Full length article

Development of a regenerative porous PLCL nerve guidance conduit with swellable hydrogel-based microgrooved surface pattern via 3D printing

Hyun Su Lee[a,b,1], Eun Young Jeon[a,1], Jae Jun Nam[c,1], Ji Hun Park[c], In Cheul Choi[c], Soo Hyun Kim[a,d], Justin J Chung[a], Kangwon Lee[e,f], Jong Woong Park[c,**], Youngmee Jung[a,g,*]

[a] Center for Biomaterials, Biomedical Research Institute, Korea Institute of Science and Technology, Seoul 02792, Republic of Korea
[b] Program in Nanoscience and Technology, Graduate School of Convergence Science and Technology, Seoul National University, Seoul 08826, Republic of Korea
[c] Department of Orthopedic Surgery, College of Medicine, Korea University, Seoul 02841, Republic of Korea
[d] NBIT, KU-KIST Graduate School of Converging Science and Technology, Korea University, Seoul 02841, Republic of Korea
[e] Department of Applied Bioengineering, Graduate School of Convergence Science and Technology, Seoul National University, Seoul 08826, Republic of Korea
[f] Research Institute for Convergence Science, Seoul National University, Seoul 08826, Republic of Korea
[g] School of Electrical and Electronic Engineering, YU-KIST Institute, Yonsei University, Seoul 03722, Republic of Korea

ARTICLE INFO

Article history:
Received 28 September 2021
Revised 13 January 2022
Accepted 18 January 2022
Available online xxx

Keywords:
PLCL nanoporous membrane
Visible light-crosslinked gelatin hydrogel
3D printing
Nerve guidance conduit
Peripheral nerve regeneration

ABSTRACT

Peripheral nerve injury causes severe loss of motor and sensory functions, consequently increasing morbidity in affected patients. An autogenous nerve graft is considered the current gold standard for reconstructing nerve defects and recovering lost neurological functions; however, there are certain limitations to this method, such as limited donor nerve supply. With advances in regenerative medicine, recent research has focused on the fabrication of tissue-engineered nerve grafts as promising alternatives to the autogenous nerve grafts. In this study, we designed a nerve guidance conduit using an electrospun poly(lactide-*co*-ε-caprolactone) (PLCL) membrane with a visible light-crosslinked gelatin hydrogel. The PLCL nanoporous membrane with permeability served as a flexible and non-collapsible epineurium for the nerve conduit; the inner-aligned gelatin hydrogel paths were fabricated *via* 3D printing and a photocrosslinking system. The resultant gelatin hydrogel with microgrooved surface pattern was established as a conducting guidance path for the effective regeneration of axons and served as a reservoir that can incorporate and release bioactive molecules. From *in vivo* performance tests using a rat sciatic nerve defect model, our PLCL/gelatin conduit demonstrated successful axonal regeneration, remyelination capacities and facilitated functional recovery. Hence, the PLCL/gelatin conduit developed in this study is a promising substitute for autogenous nerve grafts.

Statement of significance

Nerve guidance conduits (NGCs) are developed as promising recovery techniques for bridging peripheral nerve defects. However, there are still technological limitations including differences in the structures and components between natural peripheral nerve and NGCs. In this study, we designed a NGC composed of an electrospun poly(lactide-*co*-ε-caprolactone) (PLCL) membrane and 3D printed inner gelatin hydrogel to serve as a flexible and non-collapsible epineurium and a conducting guidance path, respectively, to mimic the fascicular structure of the peripheral nerve. In particular, *in vitro* cell tests clearly showed that gelatin hydrogel could guide the cells and function as a reservoir that incorporate and release nerve growth factor. From *in vivo* performance tests, our regenerative conduit successfully led to axonal regeneration with effective functional recovery.

* Corresponding author at: Center for Biomaterials, Biomedical Research Institute, Korea Institute of Science and Technology, Seoul 02792, Republic of Korea.
** Corresponding author.
E-mail addresses: ospark@korea.ac.kr (J.W. Park), winnie97@kist.re.kr (Y. Jung).
[1] These authors contributed equally to this work.

https://doi.org/10.1016/j.actbio.2022.01.042
1742-7061/

1. Introduction

The peripheral nervous system (PNS) connects the central nervous system to the entire human body, essentially processing the incoming information and controlling the sensation, motor coordination, and internal homeostasis [1]. Therefore, extensive PNS injuries caused by direct mechanical trauma, tumor extraction, and neurosurgeries cause severe loss of motor and sensory functions, putting significant physical, psychological, and economic burden on the patient [2]. Currently, autogenous grafts are used as standard reconstructive techniques for bridging such nerve defects; however, their use poses substantial limitations, such as the inevitable morbidity at the donor site, limited supply of a healthy nerve, and structural mismatch between the donor and recipient nerves [3]. Therefore, many researchers have been developing tissue-engineered nerve guidance conduits (NGCs) as promising alternatives to autografts that can bridge the gap in a transected nerve, while promoting neural regeneration [4].

Despite some benefits of the NGC systems, they still have prominent limitations regarding the extent of recovery owing to differences in the structures and components between the natural PNS and tissue-engineered NGCs [5]. Therefore, considerable efforts should be made to develop ideal regenerative NGC systems with native extracellular membrane (ECM)-like materials and biomimetic architecture for guided axonal regeneration, providing appropriate biochemical and physical cues in NGC systems. Several bioactive molecules, such as the nerve growth factor (NGF), neurotrophin-3 (NT-3), glial-derived neurotrophic factor (GDNF), and vascular endothelial growth factor (VEGF) have been introduced to enhance the nerve regenerative effects of the NGC systems [6]. From this perspective, it is important to design NGC systems to serve as reservoirs that can encapsulate the bioactive molecules at higher efficiencies, while facilitating the local sustained release of these molecules to improve the cell responses [4].

To fabricate implantable NGCs, various synthetic and natural polymers have been utilized in combination with diverse fabrication technologies, such as electrospinning, template molding, and 3D printing [7,8]. Bioabsorbable synthetic polymers, such as poly(lactic acid) (PLA) and poly(lactic-co-glycolic acid) (PLGA) are particularly employed for long-term performance *in vivo* due to their mechanical support for growing neurites and inhibition of scar tissue and appropriate biodegradation effects which enhances biocompatibility [9]. Among synthetic polymers, poly(lactide-*co*-ε-caprolactone) (PLCL) has shown promising clinical outcomes and was approved as an implantable tube by the United States Food and Drug Administration (FDA or USFDA) due to its biocompatibility, biodegradability, tailorable mechanical properties, and superior elasticity that ease the suturing process [10,11]. Natural polymers, such as collagen, fibrin, alginate, and chitosan are usually utilized as structured inner-lumen fillers due to their intrinsic nature to support cell adhesion and growth [12]. In particular, gelatin is a molecular derivative of collagen from the denaturation process, which exhibits similar molecular structures and functions as collagen [13]. Gelatin also contains a high ratio of Arg-Gly-Asp (RGD) sequences, which aid in effective cellular adhesion to the substrate as well as migration and proliferation of cells [14].

Furthermore, diverse structural guidance scaffolds, including hydrogel fillers, fibrous fillers, and patterned scaffolds with a high degree of complex organization have been designed to provide an ideal intraluminal substrate for Schwann cells (SCs), which aid in generating diffusible bioactive factors for enhanced neurite growth [15]. As SCs rely solely on the focal adhesion to the surrounding microenvironments for migration and proliferation [16], it is important to design the inner substrate of NGCs, considering suitable topography, stiffness, and diffusion behaviors that directly modulate the focal adhesion, neurite growth, and ultimate nerve repair processes.

Herein, to develop a regenerative NGC for the regeneration of the peripheral nerve, we designed electrospun PLCL nanofibers and 3D printed gelatin hydrogels as flexible epineurium and neural cell-favorable inner guidance paths, respectively. To create a gelatin-based 3D printable hydrogel, we utilized a previously reported dityrosine visible light-crosslinking system derived from insect structural proteins, such as resilin, which enabled on-demand sol-gel transition upon light irradiation [17]. Visible light-triggered crosslinking is much more biocompatible than ultraviolet (UV) light systems, owing to the presence of many molecules absorbing UV light and few visible chromophores in the cells [18]. In particular, as the hydrophilic gelatin hydrogel with RGD sequences could provide more favorable microenvironments for neural cells to adhere, migrate, and proliferate than hydrophobic PLCL membrane, this hydrogel-based anisotropic pattern can effectively support the formation of the fascicle structure composed of nerve bundles. Through optimization of the mechanical properties of PLCL nanofibers and the swelling behaviors of the gelatin hydrogels, we successfully fabricated a PLCL/gelatin conduit (PGC) with structural support and an effective inner groove micropattern to facilitate neural cell guidance. Based on the *in vivo* performance test using a rat sciatic nerve defect model, our regenerative PGCs successfully guided the regenerating axons from the proximal stump toward the distal end, avoiding unwanted results, including tube collapse during a critical recovery period and fibrous tissue ingrowth, while promoting regeneration of axons and consequent functional recovery of the nerve (Fig. 1). Additionally, we proved that the inner 3D printed gelatin hydrogel could serve as a reservoir for bioactive proteins that can be easily loaded and released *via* diffusion through hydrogel swelling and enzymatic degradation mechanisms.

2. Materials and methods

2.1. Preparation of PLCL nanoporous membrane for an epineurium of the nerve conduit

PLCL (LA:CL = 50:50) was synthesized as previously reported [19,20]. Briefly, L-lactide (LA, 100 mM; Purac Biochem, Gorinchem, Netherlands) and ε-caprolactone (CL, 100 mM; Sigma, St. Louis, MO, USA) were polymerized at 170 °C in an oil bath for 24 h with 1,6-hexanediol (0.5 mM; Sigma, St. Louis, MO, USA) as an initiator and stannous octoate (1 mM; Sigma, St. Louis, MO, USA) as a catalyst. After the reaction, the product was dissolved in chloroform (Daejung, Korea), micro-filtered, precipitated into an excess of methanol (Duksan, Korea), and then filtered and dried under vacuum. The average molecular weight (M_n) of PLCL was determined using gel permeation chromatography (GPC, Viscotek TDA 302; Malvern, UK). PLCL with M_n of 128,000 ± 15,000 g mol^{-1} was dissolved in 1,1,1,3,3,3-hexafluoroisopropanol (HFIP; TCI, Tokyo, Japan) at a concentration of 5% (w/v) and vortexed overnight.

For fabrication of the PLCL nanoporous membrane, the PLCL solution was placed in a 12 mL syringe with a metal nozzle (18G) and used for electrospinning at a voltage of 21 kV using a high-voltage power supply (NanoNC, Korea). The feed rate of the syringe pump was fixed at 0.4 mL h^{-1}, the distance between the tip of the needle and drum collector was 12 cm, and the drum collector was rotated at a speed of 100 rpm. Three PLCL membranes with different thicknesses (80, 150, and 240 μm) were obtained by varying the total volume of the PLCL solution used for electrospinning (12, 36, and 60 mL).

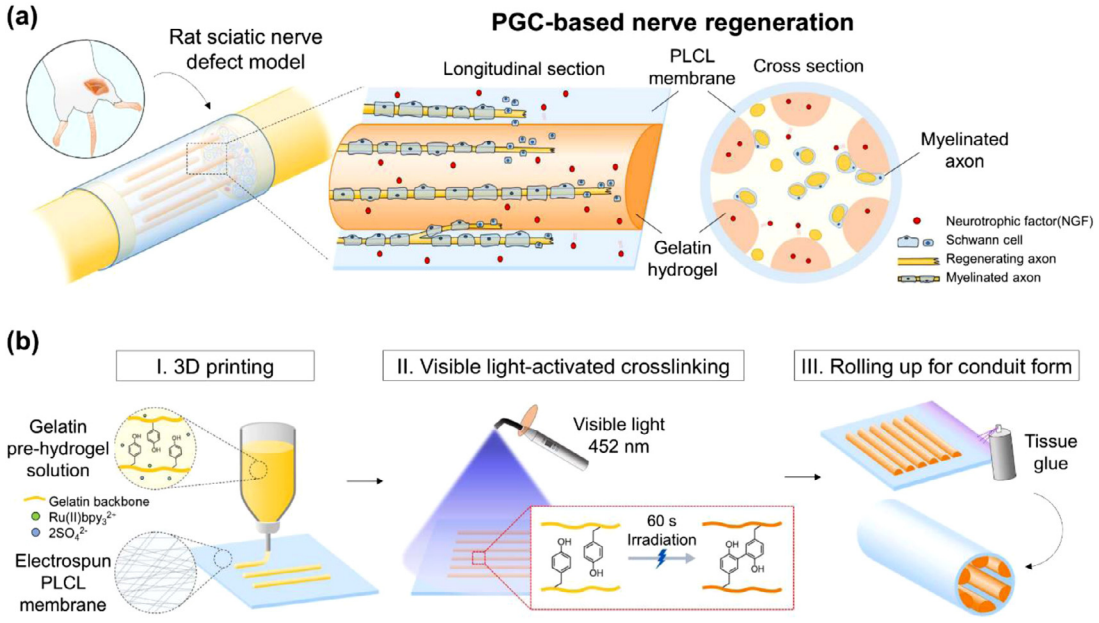

Fig. 1. *Schematic illustration for a nerve conduit consisting of PLCL and gelatin.* (a) Nerve regeneration effect of the poly(lactide-co-ε-caprolactone) (PLCL)/gelatin conduit (PGC). (b) Fabrication of the PLCL nerve conduit decorated with gelatin hydrogel-based inner guidance paths.

2.2. Preparation of visible light-crosslinked gelatin hydrogel for the inner guidance paths of the nerve conduit

The photo-crosslinked gelatin hydrogel was prepared according to a previously reported method [17]. To make a 25% (w/v) gelatin solution, 250 mg of gelatin type B powder (Sigma, St. Louis, MO, USA) was dissolved in 1 mL of phosphate-buffered saline (PBS) (Sigma, St. Louis, MO, USA) and stirred at 40 °C in a water bath overnight. Tris(2,2-bipyridyl)dichlororuthenium(II) hexahydrate ($Ru(II)bpy_3^{2+}$; Sigma, St. Louis, MO, USA) and sodium persulfate (SPS; Sigma, St. Louis, MO, USA) were used as the photoinitiator and electron acceptor, respectively, to couple two adjacent tyrosine residues of the gelatin backbone into a dityrosine adduct in the presence of visible light. To make fresh stock solutions of 25 mM $Ru(II)bpy_3^{2+}$ and 500 mM SPS, 1.85 mg of $Ru(II)bpy_3^{2+}$ and 11.9 mg of SPS were dissolved in 0.1 mL of distilled water (DW), respectively. The gelatin hydrogel was fabricated from a pre-hydrogel solution containing 25% (w/v) gelatin, 1 mM $Ru(II)bpy_3^{2+}$, and 15 mM SPS *via* blue light irradiation for 1 min using an LED dental curing lamp (460 nm, 1200 m W cm^{-2}; IBlast, Riverside, CA, USA).

For the preparation of NGF-loaded gelatin hydrogel, 700 μg of lyophilized NGF powder (Sigma-Aldrich, St. Louis, MO, USA) was dissolved in 1 mL of 10 mM sodium acetate, and then the NGF stock solution was added into the pre-hydrogel solution to achieve a final NGF concentration of 50 μg mL^{-1}.

2.3. Fabrication of a PLCL nerve conduit decorated with gelatin hydrogel-based inner guidance paths

Gelatin pre-hydrogel solution was used as a 3D printable bioink for the fabrication of inner guidance paths in a nerve conduit and prepared as explained above. The hydrogel solution (12 mL) was transferred to a NORM-JECT® Luer Lock syringe with a single plastic nozzle (27G; NanoNC, Korea). The syringe was placed in a Bio Dispenser (Dr. *In vivo*, ROKIT Inc., Korea), and one layer of a cuboid model was printed in the electrospun PLCL membrane. The cuboid model with 8 mm length, 4.7 mm width, and 1 mm height was created with Tinkercad and exported as an STL file. The STL file was then converted into a G-code file using NewCreatorK software. The printing conditions were set to a layer height of 0.02 mm, fill density of 25%, infill pattern of line, printing speed of 4 mm s^{-1}, filament diameter of 6 mm, and input flow of 140%. To avoid solidification of the gelatin pre-hydrogel solution before 3D printing, the temperature of the syringe dispenser was set to 60 °C and the temperature of the print bed was set to room temperature (RT). Following 3D printing, the printed gelatin pre-hydrogel solution was rapidly crosslinked *via* irradiation with an LED dental curing lamp at a distance of 1 cm at RT for 1 min.

A cylindrical PGC was fabricated by rolling the gelatin-printed PLCL membrane, and the end of the PLCL membrane was joined by applying a medical adhesive (Adapt 7730; Hollister, Libertyville, IL, USA) with a fine brush. The fabricated PGC had an inner diameter of 1.5 mm, a length of 12 mm, and a wall thickness (thickness of PLCL membrane) of ~240 μm.

2.4. Characterization of the PGC components

2.4.1. Electrospun PLCL nanoporous membrane

The morphology and thickness of the PLCL membranes were observed by scanning electron microscopy (SEM Inspect F; FEI company, Hillsboro, OR, USA). For SEM analysis, the samples were sputter-coated with gold, and the images were acquired at an accelerating voltage of 7 kV and a spot size of 2.5. The fiber diameter distribution and pore size of the PLCL membrane were obtained using the Image J software (National Institutes of Health, Bethesda, MD, USA).

The water permeability of the PLCL membrane was evaluated by measuring its water vapor transmission rate (WVTR). The PLCL electrospun membrane was compared with a PLCL film of the same thickness. The PLCL film was formed by spreading the PLCL solution on a petri dish and evaporating the solvent in a fume hood. Each vial filled with 5 mL of DW was sealed with a PLCL electrospun membrane and PLCL film. The sealed vials were incubated at 37 °C and the weights of the vials were measured after incubation for 1 to 7 d each. The results from at least 3 samples were averaged to obtain each measurement. The WVTR was calculated using the following equation [21]:

$$\mathrm{WVTR}\left(\mathrm{g\ m^{-2}}\right) = \frac{W_w}{A} \quad (1)$$

where W_w is the weight loss of water and A is the exposure area.

To evaluate the nutrient permeability of the PLCL membrane, the changes in the glucose concentrations in the upper and lower compartments of the PLCL electrospun membrane were measured [22]. The PLCL film was also tested as a control group. The polyester (PET) membrane of a transwell insert (Corning Inc., Corning, NY, USA) was removed and replaced with the PLCL membrane or PLCL film. 1 mL of the glucose solution of 1 mg mL^{-1}, prepared by dissolving 1 mg of glucose in 1 mL of DW, was added to the upper compartment, and 2 mL of DW was added to the lower compartment. At particular time points of 0, 1, 2, 3, 6, 12, 24, 36, and 48 h, the glucose concentration in each compartment was calculated using a glucose assay kit (Biomax, Korea). The results from at least 3 samples were averaged to obtain each measurement.

The tensile properties of the PLCL membranes with different thicknesses were measured by a universal testing machine (UTM, Instron model 5966; Instron Corp., Norwood, MA, USA) using a 1 kN load cell with a crosshead speed of 20 mm min^{-1}. According to ASTM D882-18 [23], PLCL membranes were prepared into strips with dimensions of 50 mm (length) × 10 mm (width), and the specimens were stretched until the strip ripped. The value of the tensile modulus was determined from the slope of the stress-strain curve for each specimen (20–30% strain). The results from at least 10 samples were averaged to obtain each measurement.

2.4.2. Visible light-crosslinked gelatin hydrogel

To investigate the gel content of the gelatin hydrogel formed by different SPS concentrations or different irradiation times, 50 μL of each gelatin hydrogel sample was prepared and immersed in 500 μL of DW at 37 °C for 48 h. After incubation, the supernatant containing uncrosslinked gelatin was collected, and both the hydrogel and supernatant samples were stored in a deep freezer (–70 °C). The samples were then lyophilized using a freeze dryer (FD5505; ilShin Lab Co., Ltd., Korea) overnight and weighed. The results from at least 3 samples were averaged to obtain each measurement. The gel content was calculated using the following equation [24]:

$$\text{Gel content } (\%) = \frac{W_h}{W_h + W_s} \times 100 \quad (2)$$

where W_h is the weight of the hydrogel and W_s is the weight of the supernatant after immersion.

The swelling ratio of the gelatin hydrogel was determined by measuring the weight of the swelling hydrogel at predetermined intervals. 50 μL of the gelatin hydrogel sample was prepared, weighed, and immersed in 1 mL of PBS at 37 °C. At particular time points of 0, 1, 4, 24, 48, 96, and 168 h, the sample was removed from PBS, weighed, and replaced with fresh PBS. The results from at least 3 samples were averaged to obtain each measurement. The swelling ratio was calculated using the following equation [25]:

$$\text{Swelling ratio } (\%) = \frac{W_s}{W_0} \times 100 \quad (3)$$

where W_0 is the initial weight of the hydrogel before immersion and W_s is the weight of the swollen hydrogel after each time interval.

2.4.3. PLCL nerve conduit decorated with gelatin hydrogel-based inner guidance paths

The morphologies of the flat and cylindrical PLCL membranes decorated with the gelatin hydrogel-based inner guidance paths were observed by SEM. The prepared samples were immersed in PBS at 37 °C for 24 h and washed with DW for 24 h. Then, the samples were kept in a deep freezer (–70 °C) and lyophilized using a freeze dryer overnight.

The swelling morphologies of the inner guidance paths created by the gelatin hydrogel were observed using an optical microscope (Eclipse TE2000; Nikon, Tokyo, Japan). Fabricated PGCs were cut into pieces transversely and immersed in PBS at 37 °C. At particular time intervals, the samples were removed from the PBS and the swelling morphology was observed.

2.5. In vitro *release of the encapsulated protein in light-crosslinked gelatin hydrogel*

Fluorescein isothiocyanate (FITC)-albumin was used as a model protein to evaluate the release profile of the protein encapsulated in the gelatin hydrogel. For the preparation of FITC-albumin encapsulated gelatin hydrogel, 2 mg of FITC-albumin (Sigma-Aldrich, St. Louis, MO, USA) was dissolved in 1 mL of PBS to prepare the stock solution. Then, the FITC-albumin stock solution was added into the pre-hydrogel solution to achieve a final FITC-albumin concentration of 50 μg mL^{-1}. To investigate the effect of enzymatic degradation on the release profiles, collagenase was used as an enzyme to break the peptide bonds in the gelatin hydrogel. To prepare the collagenase solution, 1.2 mg of collagenase type II (Worthington, Lakewood, NJ, USA) was dissolved in 1 mL of PBS to make the stock solution. Then, 0.5 and 0.1 U mL^{-1} of the collagenase solution were diluted and filtered with a 0.2 μm syringe filter (Adventec, Tokyo, Japan). The FITC-albumin-encapsulated gelatin pre-hydrogel solution was rapidly crosslinked *via* irradiation for 1 min with an LED dental curing lamp; 50 μL of FITC-albumin encapsulated gelatin hydrogel was incubated at 37 °C in 100 μL of PBS or 0.5 or 0.1 U mL^{-1} of collagenase solution. At particular time points of 1 to 7, and 14 d, the supernatant containing the released FITC-albumin was collected in a black 96-well plate (Thermo Fisher, Waltham, MA, USA) and replaced with fresh solutions. The fluorescence of the solution was measured by fluorescence spectroscopy (Glomax® Discover; Promega, Madison, WI, USA) using an excitation wavelength of 495 nm and an emission wavelength of 515 nm. The results from at least 3 samples were averaged to obtain each measurement. The concentration of FITC-albumin was calculated by applying the fluorescence measurement value to the standard curve, and then it was estimated as a percentage value relative to the maximum amount of FITC-albumin released.

NGF, which promotes the peripheral nerve regeneration, was selected as the target protein to be loaded into the PGC. Therefore, the release profile of NGF encapsulated in gelatin hydrogel was evaluated. To prepare the NGF-encapsulated gelatin hydrogel, 100 μg of NGF (Alomone Labs, Jerusalem, Israel) was dissolved in 100 μL of DW to prepare the stock solution. The NGF stock solution was added to the pre-hydrogel solution to achieve a final NGF concentration of 50 μg mL^{-1}. The collagenase solution was prepared as previously described. 50 μL of NGF-encapsulated gelatin hydrogel was incubated at 37 °C with 100 μL of 0.1 U mL^{-1} of collagenase solution and PBS. At particular time points of 1, 4, 7, 14, 21, 28, 38, 48, and 58 d, the supernatant was collected, kept in a deep freezer (–70 °C) for later analysis, and replaced with fresh solutions. The amount of NGF released was analyzed using an enzyme-linked immunosorbent assay (ELISA) kit (Invitrogen, Waltham, MA, USA). The results from at least 5 samples were averaged to obtain each measurement.

2.6. In vitro *SH-SY5Y cell study*

The human neuroblastoma SH-SY5Y cell line was purchased from the Korean Cell Line Bank(Korea). Cells were cultured in the Dulbecco's modified Eagle's medium (DMEM)/F-12 medium (Gibco, St. Louis, MO, USA) supplemented with 10% fetal bovine serum (FBS; HyClone, Logan, UT, USA) and 1% penicillin-streptomycin (Gibco, St. Louis, MO, USA) at 37 °C in a humidified atmosphere of 5% (v/v) carbon dioxide (CO_2). At a confluency of 80–90%, the cells were treated with 0.25% trypsin-ethylenediaminetetraacetic

acid (EDTA) (Thermo Fisher, Waltham, MA, USA) and seeded onto the samples at a density of 10^4 cells cm^{-2} and cultured with the growth medium. For the experimental groups, the PLCL membrane alone and the PLCL membrane printed with the gelatin hydrogel or the NGF-loaded gelatin hydrogel were prepared and cut into 8 mm squares for *in vitro* cell studies. Prior to cell seeding, the samples were immersed in 70% ethanol solution, sterilized under ultraviolet (UV) light for 1 h, and then washed with PBS for 24 h at 37 °C.

Cell viability was visualized using a live/dead staining kit (Thermo Fisher, Waltham, MA, USA). After 1, 3, and 7 d of cell seeding, the samples were washed with PBS and incubated with 2 μm of calcein acetoxymethyl (AM) and 4 μm of ethidium homodimer-1 for 1 h at 37 °C. The stained samples were observed using a confocal laser scanning microscope (CLSM, LSM700; Zeiss, Jena, Germany).

Cell adhesion and proliferation abilities were determined using the Cell Counting Kit-8 (CCK-8; Dojindo, Rockville, MD, USA). After 1, 3, and 7 d of cell seeding, the reagents were added to each well and incubated at 37 °C for 3 h according to the manufacturer's protocol. Absorbance at 450 nm was measured using a microplate reader (VersaMax; Molecular Devices, San Jose, CA, USA). The results from at least 8 samples were averaged to obtain each measurement.

The morphologies and neurite outgrowths of SH-SY5Y cells in the samples were monitored using immunofluorescence staining. After 1, 3, and 7 d of cell seeding, the samples were fixed in 4% formaldehyde (Biosesang, Korea) at 4 °C overnight and permeabilized in PBS with 0.1% Triton X-100 (Biosesang, Korea) at RT for 5 min. The samples were then incubated with β-tubulin antibody with Alexa Fluor 488 (1:100, 2G10-TB3; Invitrogen, Waltham, MA, USA) and F-actin antibody with Alexa Fluor 594 (1:400, A12381, Invitrogen, Waltham, MA, USA) at RT for 1 h. The samples were mounted using an anti-fade mounting medium with 4′, 6-diamidino-2-phenylindole (DAPI) (Vectashield; Vector Laboratories, Burlingame, CA, USA) and observed using CLSM. At least 3 samples with 100 cells per sample were counted using the Image J software to measure the ratio of cells that showed neurite outgrowths. Cells with neurites longer than the diameter of the cell body were counted as differentiated cells. To measure the neurite length of differentiated cells incubated on the PLCL membrane or gelatin hydrogel, at least 3 samples with 100 cells per sample were counted using the Image J software.

2.7. In vivo *rat sciatic nerve defect model*

2.7.1. *Experimental animals and surgical procedures*

All animal experiments were conducted on male Lewis rats weighing 250–300 g according to the recommendations of the Guideline of Association for Assessment and Accreditation of Laboratory Animal Care International (AAALAC International) and approved by the Institutional Animal Care and Use Committee of the Korea University College of Medicine (IACUC Approval no. 2020-0153). A total of 33 male Lewis rats were randomly assigned to three experimental groups and repaired as follows: autograft (autograft group, $n = 11$), PLCL conduit with 3D printed gelatin hydrogel (PGC group, $n = 11$), and PLCL conduit with 3D printed NGF-loaded gelatin hydrogel (PGC-NGF group, $n = 11$). The animals were anesthetized *via* isoflurane inhalation. The left sciatic nerve of each animal was exposed at the mid-thigh level from the inferior margin of the piriformis muscle approximately 5 mm distal to the bifurcation. A uniform 8 mm-long segment of the sciatic nerve was excised at the midportion of the sciatic nerve with sharp microsurgical scissors under an operating microscope. The excised nerve segment between the proximal and distal stumps was reversed and repaired using five 10-0 epineurial interrupted sutures (Ethilon®; Ethicon Inc., Somerville, NJ, USA) at each end of the stump in animals in the autograft group. For the PGC and PGC-NGF groups, each 12 mm sized NGC with 3D printed gelatin hydrogel and NGF-loaded gelatin hydrogel was inserted between the proximal and distal stumps using five 10-0 epineurial interrupted sutures at each stump, while the ends of each stump were inserted into the conduit sleeve about 2 mm from each end to create a uniform 8 mm nerve defect. The skin was repaired using 4-0 interrupted sutures (Ethilon®; Ethicon Inc., Somerville, NJ, USA). The contralateral (right) side of the sciatic nerve was left intact to serve as an intra-individual control. All animals were housed in a group of three in a temperature- and humidity-controlled environment with a 12 h light/dark cycle and ad libitum access to food and water. During the 12-week observation period, survival measurements of the video-gait analysis were made every three weeks. Non-survival measurements, including maximum isometric tetanic force, muscle weight ratio, and histological analysis, were performed at 6 weeks and 12 weeks.

2.7.2. *Sample preparation for* in vivo *rat study*

The PLCL membrane and the materials for the inner guidance paths were sterilized using ethylene oxide (EO) gas (Person EO-35L; Person Medical Co., Ltd., Korea). The 3D printer was sterilized under UV light for 1 h in 70% ethanol solution. After 3D printing, the conduit was fabricated on a clean bench. The fabricated PGC had an inner diameter of 1.5 mm and a length of 12 mm. Finally, the prepared PGC and PGC-NGF were sterilized under UV light for 1 h and stored in humidified conditions at 4 °C for implantation.

2.7.3. *Assessment of functional motor recovery*

Video gait and ankle angle analyses

To assess the serial functional recovery after the operation, the active ankle angle at terminal stance (ATS) was measured every three weeks for up to 12 weeks, as the angle in the gait cycle has been shown to correlate most accurately with functional recovery [26]. At weeks 3 and 6, all animals from each group were subjected to the measurements. At 9 and 12 weeks, seven animals from each group underwent the measurement and four animals from each group underwent non-survival measurements at week 6.

To obtain the gait analysis video, a walking treadmill was used with a 20 cm-high transparent Plexiglas, which was 48 cm long and 10 cm wide attached on both sides. It was gradually accelerated to 20 cm s^{-1}, allowing the animal to walk in a straight forward direction. Images were acquired with a 60 Hz digital camera positioned at a distance of 1 m. Three satisfactory trials per animal were obtained by separate repeated recordings. The frame of the video at the toe-off, that is, the moment of maximal plantar flexion of the experimental side ankle joint, was selected, and the leg segment and the foot segment were manually identified for the terminal stance phase. The angle between the longitudinal axes of the tibia and foot segment was measured from still images using the Image J software.

Maximum isometric tetanic force

To evaluate the reproducible quantitative motor recovery, the maximum isometric tetanic force of the tibialis anterior (TA) muscles of the Lewis rats was measured. Four animals from each group were sacrificed at week 6 to observe their midpoint functional recovery. The TA of the remaining animals (7 from each group) was measured at 12 weeks using the previously described method [27].

The TA tendon insertion site was exposed and released from the extensor retinaculum. The hind limb was stabilized with two 0.035 inch Kirschner wires placed at the distal femur and distal tibia on a wooden platform. The exposed TA tendon was tied with a black silk thread, and the other end of the black silk thread was connected to an isometric force transducer (Harvard Apparatus, Holliston, MA, USA). The signal was processed on a computer using LabScribe software (Iworx/CB Sciences, Dover, NH, USA). Two small,

custom-made hook-shaped bipolar stimulating electrodes, using a CK-1 field stimulator (CB Science, Escondido, CA, USA), were placed at the sciatic nerve proximal to the graft site. Equal stimulation pulses were applied to all the measurements: preload of 10 g, stimulus intensity of 10 V, pulse duration of 2 ms, and pulse frequency of 100 Hz. The stimulations were applied five times, and to avoid muscle fatigue, the TA muscle was rested for two min between the stimulations with no preload. The highest force was selected and determined as the maximum isometric tetanic force. An identical procedure was performed on the contralateral normal leg.

Muscle weight ratio

To obtain the weight of the tibialis anterior muscle, the animals were sacrificed after the completion of the muscle tetanic force measurement. Due to peripheral nerve injury, the muscle was denervated with a subsequent tendency of muscle atrophy. The muscle was carefully dissected from the surrounding tissues and weighed in grams. The same procedure was performed on the contralateral side, and the weight was normalized using data from the contralateral side and reported as a percentage of the normal contralateral side.

2.7.4. Histological analyses

The nerve segment 5 mm distal from the distal suture site was utilized for cross-sectional histological analysis to evaluate the final result of axonal regeneration. Each specimen was fixed with 2.5% glutaraldehyde (Sigma, St. Louis, MO, USA) in 0.1 mol L^{-1} PBS for 48 h at room temperature and post-fixed with 1% osmium tetroxide (Sigma, St. Louis, MO, USA). It was then embedded in an epoxy resin (Sigma, St. Louis, MO, USA), cut into 1 μm semithin sections with an ultramicrotome (Leica, Wetzlar, Germany), and stained with 1% toluidine blue for light microscopy (BX46, Olympus, Tokyo, Japan). A charge-coupled device camera (DP21, Olympus, Tokyo, Japan) was used to digitalize the images, which were analyzed using standard image processing at a magnification of × 20. The tibial nerve cross-section was analyzed using Image J software. The total number of myelinated axons, myelinated fiber area, nerve fiber density, N ratio, myelin thickness, and G ratio were determined for specimens obtained at 12 weeks from seven animals in each group. The nerve fiber density was calculated by dividing the number of myelinated axons counted in the selected area by the size of the area. The N ratio was calculated as the total myelinated fiber area divided by the total tissue cable area. The G ratio was calculated as the axon diameter divided by total fiber diameter. More detailed histomorphometric methods for measurements of these parameters are described in **Fig. S5**. All parameters were analyzed at × 60 magnification, and averaged from five different views obtained by random sampling. This represents information regarding the number of sprouting events [28].

The autograft and regenerated nerve tissues with the surrounding PGC were harvested to evaluate their nerve regeneration capacities. Four specimens from each experimental group at 6 and 12 weeks were fixed with 4% formaldehyde, immersed in cryo-embedding media (Tissue-Tek® O.C.T. Compound; Sakura Finetechnical Co., Tokyo, Japan), and frozen immediately at –20 °C. Then, the specimens were cut into longitudinal sections of 10 μm thickness on poly l-lysine-coated slides. Tissue sections were stained with hematoxylin-eosin (H&E) and Masson's trichrome (MT) and analyzed under a light microscope (Eclipse TE2000; Nikon, Tokyo, Japan). To compare the cross-sectional collagen area among three experimental groups, the percentage of collagen area from MT stained images was measured using Image J software. The results from at least 3 samples were averaged to obtain each measurement.

For immunohistochemical staining, S-100 and β-tubulin were used as specific markers for Schwann cells and neurons, respectively. The sectioned specimens were incubated with primary S-100 antibody (1:100, ab52642; Abcam, Cambridge, UK) and β-tubulin antibody with Alexa Fluor 488 (1:100, 2G10-TB3; Invitrogen, Waltham, MA, USA) overnight at 4 °C. The specimens were then incubated with the secondary antibody Alexa-594 anti-mouse IgG (1:1000, ab150128; Abcam, Cambridge, UK) at RT for 1 h. The nuclei were counterstained with anti-fade mounting medium with DAPI (Vector Laboratories, Burlingame, CA, USA), and the stained specimens were observed using CLSM. To compare the relative fluorescence intensity among three experimental groups, the value from immunohistochemical stained images was measured using Image J software. The results from at least 3 samples were averaged to obtain each measurement.

2.8. Statistical analysis

Statistical analysis was performed using two-way analysis of variance (ANOVA). The Kolmogorov-Smirnov test was used to determine the normality of the distributions, and the Kruskal-Wallis test, with the *post hoc* Mann-Whitney test, was used to determine the differences in the functional and histomorphometric parameters between the groups. The data are shown as the mean ± standard deviation (SD), and the level of significance was set at $P < 0.05$. Statistical analyses were performed using the SPSS software v.20 (IBM, Armonk, NY, USA).

3. Results and discussions

3.1. Preparation of PGC

3.1.1. Non-collapsible PLCL membrane with high permeability

To create the highly elastic outer membrane of peripheral nerves, a PLCL nanoporous membrane, an epineurium that mechanically protects the interior surface of the nerve, was obtained by electrospinning. SEM analysis revealed that the fiber diameter and pore size of the PLCL membrane were 649 ± 102 nm and 4.9 ± 1.7 μm, respectively (Fig. 2**a**). According to previous studies, the optimal pore size for nerve conduits is in the range of 5–30 μm to enable the diffusion of nutrients and wastes [29–32]. However, wall pores larger than 10 μm can induce the infiltration of non-neural cells into the conduit lumen, thus obstructing the neurite outgrowth and subsequent axonal regeneration [33,34]. Furthermore, the suitable permeability of electrospun PLCL for water vapor and nutrients to enable the diffusion of nutrients and wastes was verified through WVTR measurement and a glucose transfer assay, respectively (Fig. 2**b** and **c**). The WVTR results showed that the rate of the PLCL membrane (4085 ± 257 g m^{-2}) was higher than that of the PLCL film (758 ± 43 g m^{-2}) at all time intervals. In addition, from the glucose transfer assay, it was found that in the PLCL electrospun membrane group, glucose concentration in the lower compartment increased steadily from 0.9 ± 0.1 μmol mL^{-1} until 4.9 ± 0.2 μmol mL^{-1}. In case of the PLCL membrane with the gelatin hydrogels, there was no significant difference in the glucose permeability of PLCL membrane group (data not shown). Based on this result, we verified that gelatin hydrogels do not affect the nutrient permeability of the PLCL membrane. However, the PLCL film group showed no significant difference in glucose concentration in the lower compartment after 48 h of experiment (0.7 ± 0.5 μmol mL^{-1}) when compared with the initial state (0.7 ± 0.05 μmol mL^{-1}). This might be because of the nanoporous structure of the PLCL membrane, facilitating high water vapor and nutrient permeability.

Ideally, a nerve conduit should exhibit mechanical properties similar to those of native nerve tissue to endure manual manipulation, such as suturing during implantation and *in vivo* physiological loading without tube collapse after implantation [35,36]. To optimize the mechanical characteristics of the PLCL membrane,

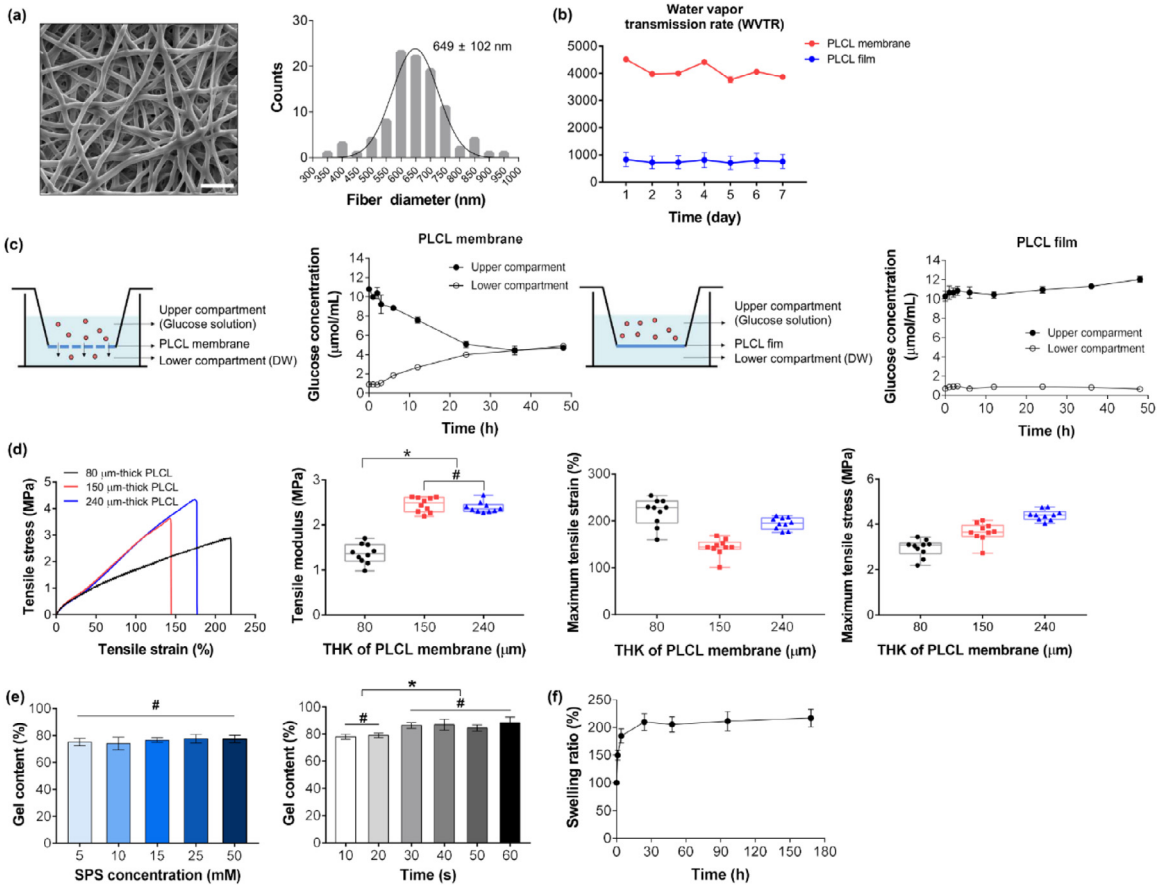

Fig. 2. *Characterization of the PLCL membrane and light-crosslinked gelatin hydrogel.* (a) Scanning electron microscopy (SEM) image of the PLCL membrane and the fiber diameter distributions with average fiber diameter. Scale bar = 5 μm. (b) Water vapor transmission rate (WVTR) was determined by measuring the changes in the weights of the vials filled with 5 mL of distilled water (DW), sealed with the PLCL membrane and PLCL film, and incubated at 37 °C ($n = 3$). (c) Nutrient permeability of the PLCL membrane was evaluated using a glucose transfer assay. Glucose concentration in the upper and lower compartments of the PLCL membrane and PLCL film was evaluated at particular time intervals using the glucose assay kit ($n = 3$). (d) Mechanical properties of the PLCL membranes with different thicknesses (80, 150, and 240 μm) ($n = 10$). (e) Gel content of the gelatin hydrogels with different SPS concentrations and irradiation times (n ≥ 3) (*$P < 0.05$ and #$P > 0.05$). (f) Dynamic kinetics of the swelling ratio of the gelatin hydrogel ($n = 3$).

we fabricated three PLCL membranes of different thicknesses by varying the total volume of the PLCL solution (12, 36, and 60 mL) for electrospinning and conducted tensile tests (Fig. 2**d**). The membrane thickness increased with increasing the volume of the PLCL solution, and the thickness was 80, 150, and 240 μm, respectively. There was no significant difference in the tensile modulus between the 150 μm-thick (2.5 ± 0.2 MPa) and 240 μm-thick PLCL membranes (2.4 ± 0.1 MPa). Their values were higher than that of 80 μm-thick PLCL (1.4 ± 0.2 MPa) and the tensile modulus at all thickness levels was in the range of the rat sciatic nerve's value (0.6 ± 0.2 ~ 13.8 ± 5.5 MPa) [37,38]. The maximum strain value was highest in the order of 80 μm-thick (219 ± 28%), 240 μm-thick (195 ± 12%), 150 μm-thick (144 ± 17%) PLCL membranes, and the rat sciatic nerve (0.8 ± 0.1 ~ 49.2 ± 2.4%) [37,38]. The maximum stress value was increased as the thickness of PLCL membrane increased (3 ± 0.4, 3.7 ± 0.4, and 4.4 ± 0.2 MPa for 80 μm-thick, 150 μm-thick, and 240 μm-thick PLCL membranes, respectively), and the maximum stress value at all thickness levels was in the range of the rat sciatic nerve's value (2.7 ± 1 ~ 6.1 ± 1.5 MPa) [37,38]. The 80 μm-thick PLCL membrane showed the maximum strain value owing to its stretchability resulting from its thin thickness; however, it collapsed when fabricated into a conduit shape because of its low mechanical strength **(Fig. S1)**. As a result, a 240 μm-thick PLCL membrane was utilized for the epineurium of PGC because it showed proper mechanical strength and elasticity matching to the rat sciatic nerve. Therefore, we expected that 240 μm-thick PLCL membrane could endure stress during operation and support nerve regeneration through PGC by reducing the risk of collapse.

3.1.2. 3D printable light-crosslinked gelatin hydrogel for inner guidance paths

To create the inner guidance paths for the PGC with 3D printing, gelatin was utilized for a previously visible light-crosslinked dityrosine crosslinking system [17]. By adopting the photocrosslinking system, we gained advantages such as dityrosine crosslinks-inherent conformational stability, flexibility [39], and on-demand rapid crosslinking within 60 s *via* blue light irradiation. Gelatin, which is derived from collagen by acidic or basic hydrolysis, has a similar composition to collagen; additionally, they have similar desirable properties, such as biocompatibility and possible degradation by collagenase *in vivo* [40–42]. RGD peptides of gelatin can accelerate SC migration and proliferation to regenerate nerves [13].

To enhance crosslinking efficiency while maintaining 3D printability, we used a high concentration of gelatin (25% (w/v)). At concentrations above 25% (w/v), needle clogging occurred during 3D printing because of its high viscosity. $Ru(II)bpy_3^{2+}$ was set to a low concentration of 1 mM because this catalyst circulates during the photochemical reaction. To optimize the concentration of the electron acceptor (sodium persulfate; SPS) and irradiation time, we measured the gel content of several hydrogels prepared with vari-

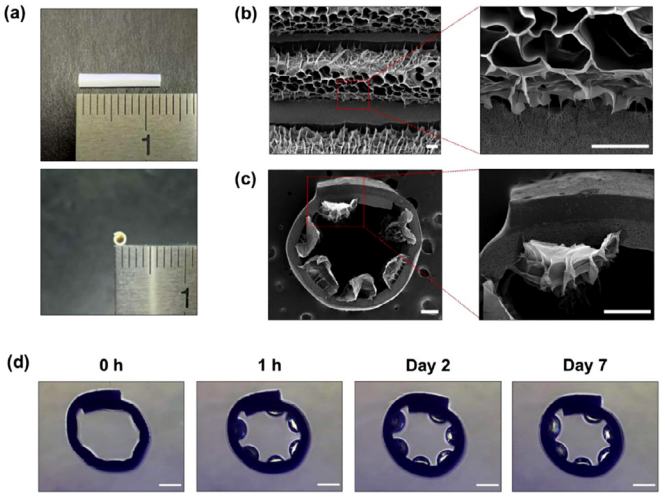

Fig. 3. *Characterization of the fabricated PGC.* (a) The length and the diameter of the PGC. (b) SEM images of the PLCL membrane with the 3D printed gelatin hydrogel after incubation in phosphate-buffered saline (PBS) at 37 °C. Scale bar = 100 μm. (c) SEM images of the PLCL nerve conduit cross-section with the 3D printed gelatin hydrogel after incubation in PBS at 37 °C. Scale bar = 200 μm. (d) Optical images of the swelling morphologies of the cross-sectioned PGC in PBS at 37 °C. Scale bar = 500 μm.

ous SPS concentrations and irradiation times. There was no significant difference in gel content between the hydrogels with SPS concentration of 5 mM to 50 mM (76.2 ± 1.4%) and irradiation time of 30 s to 60 s (86.6 ± 1.4%). Therefore, 15 mM of SPS concentration and irradiation time of 60 s were used for gelatin crosslinking, as described in a previous study (Fig. 2**e**) [17]. Through optimization, a 3D printable gelatin pre-hydrogel solution was obtained and rapidly crosslinked into a hydrogel *via* visible light.

Generally, gelatin hydrogels exhibit swelling behavior by absorbing water through hydrogel bonds between hydrophilic moieties [43]. To characterize the water absorption of our light-crosslinked gelatin hydrogel, the swelling ratio was estimated (Fig. 2**f**). After 24 h of swelling in PBS, the swelling ratio of the gelatin hydrogel reached 209 ± 12% and was maintained for 7 days. In the process of fabricating the PGC, the swelling behavior of the inner hydrogel path is one of several important factors to be considered for the formation of an effective microgrooved surface pattern, because neuronal cells infiltrate and migrate through guidance paths for effective axonal regeneration.

The creation of inner guidance paths with gelatin pre-hydrogel by 3D printing proceeded by stacking layer by layer. To optimize the number of stacking layers, PGCs with different heights of the inner gelatin hydrogel were fabricated and immersed in PBS at 37 °C. After immersion, one layer of inner guidance paths showed the most ideal swelling image, providing sufficient space between the paths. In the case of PGCs with more than two layers of gelatin hydrogel, excessive swelling led to an ungrooved surface pattern **(Fig. S2a)**. PGCs with 6 to 10 layers showed the opening of the conjugated conduit due to the dramatic swelling behavior of the inner gelatin hydrogel **(Fig. S2b)**. Therefore, we printed one layer of the gelatin hydrogel on the PLCL membrane to generate uniform inner guidance paths of the nerve conduit.

3.2. Characterization of PGC

For fabrication of the cylindrical PGC, the PLCL membrane decorated with gelatin-based 3D printed hydrogels was manually rolled and finished with the bioadhesives. The PGC had a length of 12 mm and an inner diameter of 1.5 mm (Fig. 3**a**). SEM analysis verified the uniform 3D printed inner hydrogel paths on the PLCL membrane, creating a microgrooved surface pattern to serve as a guidance path for neural cells (Fig. 3**b** and **c**). Compared with the PLCL membrane, the 3D printed gelatin hydrogel showed an interconnected pore structure with a relatively large pore size (71 ± 27 μm), which allowed easy encapsulation and delivery of cells and bioactive molecules and facilitated neural cell infiltration and migration [44]. To monitor the swelling behavior of the inner hydrogel paths in the PGC, the cross-sectioned PGCs were incubated in PBS at 37 °C. The PGC displayed selective swelling of the inner paths within 1 h; it lasted for 7 days (Fig. 3**d**). During swelling in PBS, inner gelatin hydrogels remained in place without delamination from PLCL membrane due to possible interfacial adhesion between gelatin and PLCL such as mainly hydrophobic interaction and hydrogen bonding. Based on this result, it was expected that the 3D printed gelatin hydrogel paths could serve as a guide for nerve regeneration through the PGC.

To determine the release kinetics of encapsulated proteins from gelatin hydrogel, FITC-albumin as a model protein was simply encapsulated in the gelatin hydrogel *via* photocrosslinking. FITC-albumin-loading gelatin hydrogels were incubated in PBS with or without collagenase to investigate the effect of the degradability of the gelatin hydrogel on its release profile of the encapsulated protein. The hydrogel in PBS showed sustained release of the encapsulated protein for up to 14 days by diffusion from the porous structure of the gelatin hydrogel. As expected, the hydrogel in PBS with collagenase showed a much higher release rate than that without collagenase possibly due to gradual collapse of the gelatin hydrogel structure by enzymatic degradation in the former (Fig. 4**a**). NGF has been also loaded as a target bioactive protein to support the survival and differentiation of neurons [45]. To determine the amount of released NGF, ELISA was performed using the supernatants after hydrogel incubation in PBS. We found that NGF was continuously released from the gelatin hydrogel over 58 days. At 58 days, the cumulative amount reached 57.4 ± 5.5 ng (Fig. 4**b**). These results implied that the light-crosslinked gelatin hydrogel could serve as a vehicle for the encapsulation and release of bioactive molecules by simultaneous diffusion through swelling and enzymatic degradation.

3.3. Evaluation of the in vitro SH-SY5Y cell study

The cytocompatibility of PGC was examined using human neuroblastoma SH-SY5Y cells, which are known to differentiate into a mature neuron-like phenotype by growth factors such as NGF [46]. SH-SY5Y cells were cultured on different experimental surfaces, including PLCL membrane (PLCL) and PLCL membrane printed with gelatin hydrogel (PLCL-gelatin) or NGF-loaded gelatin hydrogel (PLCL-gelatin/NGF) for 7 days. From live/dead stained images, cells seeded on all experimental groups showed strong green fluorescence and weak red fluorescence, which can be interpreted as high viability, and the green fluorescent live cells gradually increased with time. In particular, the area of the PLCL membrane printed with hydrogel showed a higher density of green fluorescence compared to the area of only the PLCL membrane at all time points. This indicates that the gelatin hydrogel provided a more favorable environment for SH-SY5Y cells to adhere and proliferate on the substrate effectively (Fig. 5**a**). The CCK-8 assay revealed that the optical density (OD) value of each experimental group increased with time. There was no significant difference in cell adhesion and proliferation between the PLCL-gelatin (0.06 ± 0.002) and PLCL-gelatin/NGF (0.06 ± 0.007) groups. However, their values were markedly higher than those of the PLCL group (0.04 ± 0.002), which corresponded to the results of live/dead staining (Fig. 5**b**). We believe that the cytocompatibility of PGC was attributed to the use of cell-favorable biomaterials, such as PLCL and gelatin, and a non-cytotoxic crosslinking system using visible light.

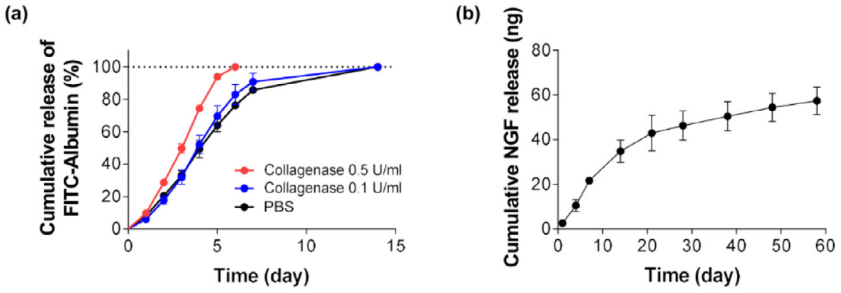

Fig. 4. *In vitro release profiles of the encapsulated protein in light-crosslinked gelatin hydrogel.* (a) The released fluorescein isothiocyanate (FITC)-albumin was detected by fluorescence spectroscopy ($n = 3$). (b) The released nerve growth factor (NGF) was detected by the enzyme-linked immunosorbent assay (ELISA) ($n = 5$).

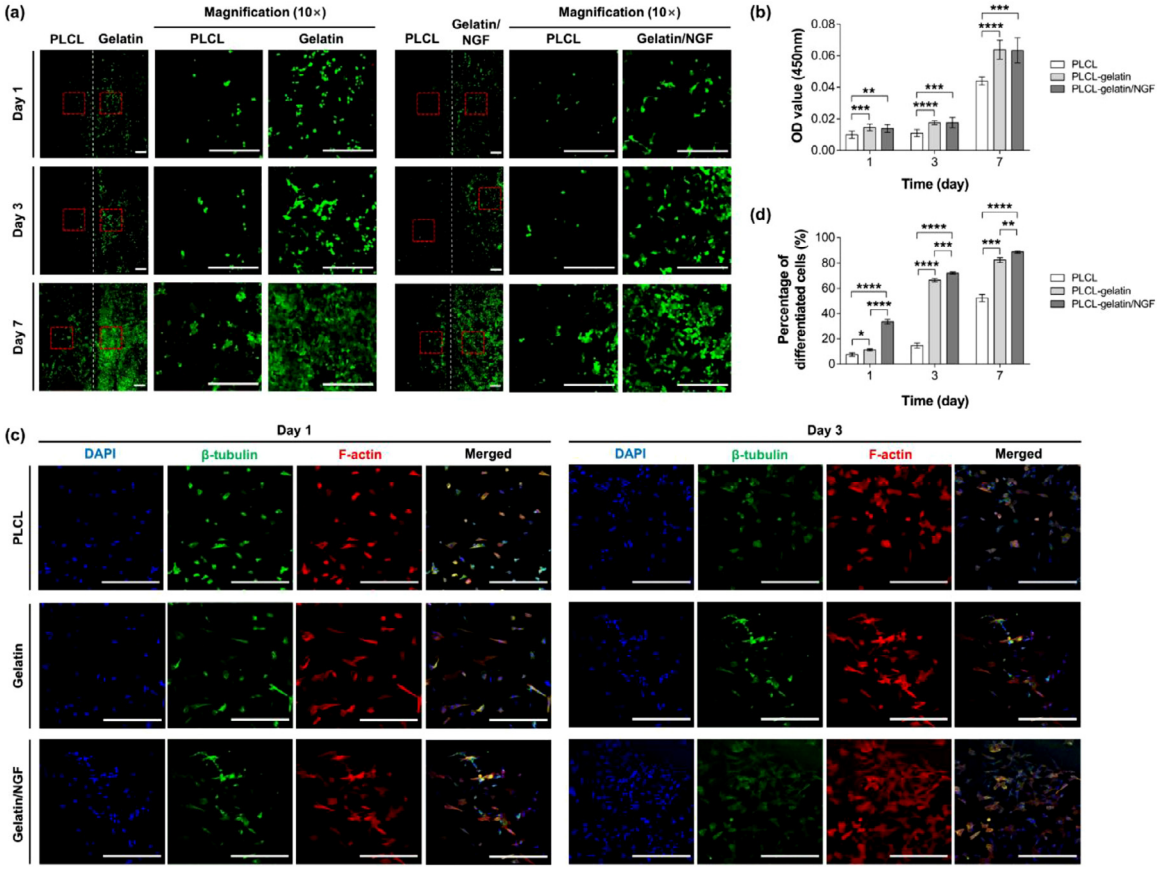

Fig. 5. *In vitro study of the SH-SY5Y cells.* (a) Cell viability test was performed with the live/dead assay using calcein-acetoxymethyl (AM)/ethidium staining. The cells were incubated on PLCL-gelatin and PLCL-gelatin/NGF and tested at 1, 3, and 7 d after cell seeding. Scale bar = 300 μm. (b) Cell cytotoxicity test was performed using the Cell Counting Kit-8 (CCK-8) assay. Cells were incubated on PLCL, PLCL-gelatin, and PLCL-gelatin/NGF and tested at 1, 3, and 7 d after cell seeding ($n = 8$). (c) Immunofluorescence staining of cells with 4′, 6-diamidino-2-phenylindole (DAPI) (blue), β-tubulin (green), and f-actin (red) after incubation on PLCL, PLCL-gelatin, and PLCL-gelatin/NGF for 1 and 3 d. Scale bar = 300 μm. (d) Quantitative analysis of the percentage of differentiated cells by counting the number of cells with neurites having diameters longer than the diameter of the cell body ($n = 3$). ($^*P < 0.05$, $^{**}P < 0.01$, $^{***}P < 0.001$, and $^{****}P < 0.0001$) PLCL: PLCL membrane only; PLCL-gelatin: PLCL membrane with gelatin hydrogel; PLCL-gelatin/NGF: PLCL membrane with NGF-loaded gelatin hydrogel.

Cell adhesion to neighboring substrates plays an important role in the nerve regeneration process at the injured site by promoting neurite outgrowth, myelination, and neuronal differentiation. To investigate the focal adhesion and morphology of the cells, F-actin and β-tubulin staining was performed. Interestingly, the results showed that more cells were initially adhered to the PLCL membrane printed with gelatin hydrogel or NGF-loaded gelatin hydrogel compared to the PLCL membrane, and proliferated over time. In addition, there were morphological differences between PLCL membranes printed with hydrogel and PLCL membranes. Cells on PLCL membrane printed with hydrogel showed typical neuronal morphology of slender shape and neuronal processes [47], while cells on the PLCL membrane showed a relatively short slender shape. In particular, F-actin staining demonstrated that the gelatin hydrogel or NGF-loaded gelatin hydrogel allowed more focal adhesion of cells compared to the PLCL membrane (Figs. 5**c and S3**). The reason might be the hydrogel-inherent hydrophilic environment favorable for cellular activities. Owing to their highly hydrated environments, hydrogels have common merits such as good biocompatibility, high permeability for oxygen, nutrients, and other water-soluble metabolites, and soft tissue-like viscoelastic properties compared to other types of polymeric biomaterials [48]. In particular, gelatin used in this work retains informational signals such as the RGD sequence, a particular integrin joint location for cellular focal adhesion [14,49,50], which could contribute to better cell adhesion and migration on our gelatin hydrogel than

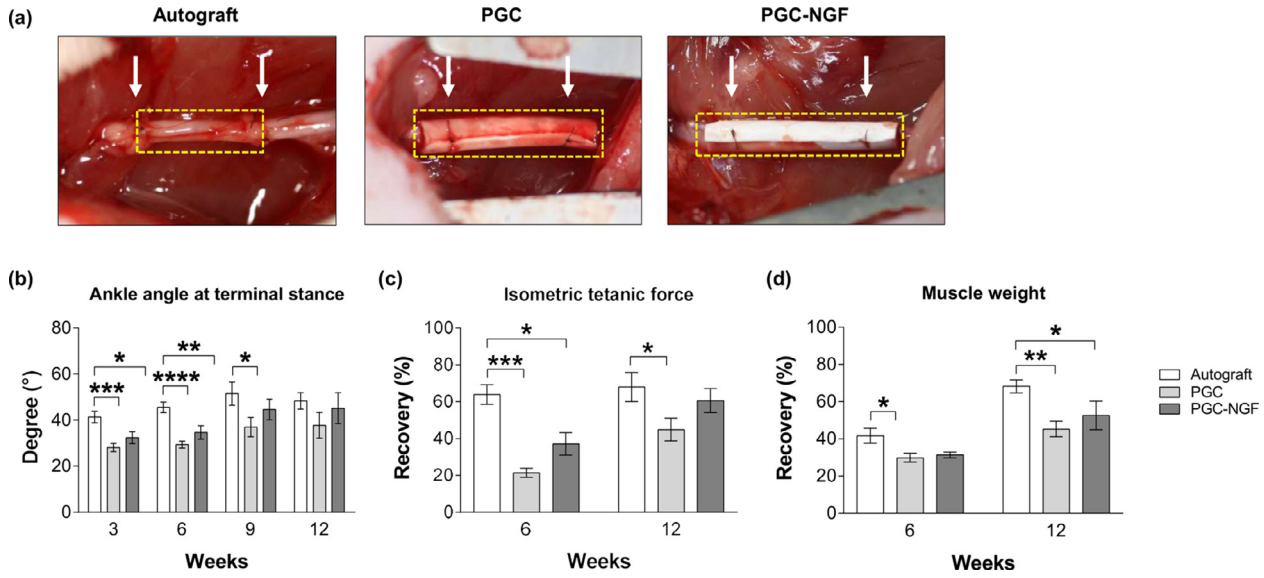

Fig. 6. *Results of surgical procedure and evaluation of the functional motor recovery of the in vivo rat sciatic nerve defect model.* (a) Images of the autograft and implantation of PGC and PGC-NGF after the operation. The suture parts (white arrows) and grafts including autologous sciatic nerve and PGCs (yellow dashed region) are indicated. (b) Active ankle angle at the terminal stance of all experimental groups measured at 3, 6, 9, and 12 weeks after the operation ($7 \leq n \leq 11$). (c) Maximum isometric tetanic force measured at 6 and 12 weeks after the operation ($4 \leq n \leq 7$). (d) Muscle weight ratio of the tibialis anterior muscle measured at 6 and 12 weeks after the operation ($4 \leq n \leq 7$) ($^{*}P < 0.05$, $^{**}P < 0.01$, $^{***}P < 0.001$, and $^{****}P < 0.0001$). PGC: PLCL conduit with 3D printed gelatin hydrogel; PGC-NGF: PLCL conduit with 3D printed NGF-loaded gelatin hydrogel.

hydrophobic PLCL membrane [51]. Moreover, based on cell morphology, we determined the degree of differentiation of SH-SY5Y cells into mature human neurons by counting the number of cells with neurites longer than the diameter of the cell body diameter. Cells seeded on PLCL membrane with NGF-loaded gelatin hydrogel showed significantly higher neurogenic differentiation (88.7 ± 0.7%) than cells on PLCL membrane (52.2 ± 2.3%) and PLCL membrane with gelatin hydrogel (82.3 ± 1.6%) (Fig. 5**d**). This result is due to the fact that NGF is a neurotrophic factor responsible for neuronal survival and differentiation [44]. Furthermore, from measurement of the average neurite length of differentiated cells **(Fig. S4)**, it was found that on both day 1 and 3, the average value on gelatin hydrogel (26.8 ± 0.8 and 45.2 ± 2.1 μm) was slightly higher than on the PLCL membrane (23.2 ± 0.4 and 42 ± 1.4 μm). On day 7, it was difficult to clearly monitor neurite outgrowth because proliferated cells formed cluster. These results indicated that 3D printed gelatin hydrogel paths could effectively guide cells and that the release of NGF from PGC-NGF retained its bioactivity.

3.4. Evaluation of the functional motor recovery of the in vivo *rat model*

3.4.1. General observation following surgery and weight gain

After the surgical procedure (Fig. 6**a**), the weight and mobility of all animals showed progressive gain. At week 12, the mean percentage of animal weight compared to the weight at the time of surgical procedure in the autograft group was 122%. That of the PGC group was 117% and that of the PGC-NGF group was 103%. None of the animals showed any other complications such as infection, delayed wound healing, or signs of auto-mutilation. Also, none of the animals showed macroscopic signs of graft disconnection or serious neuroma formation.

3.4.2. Ankle angle at terminal stance (ATS) measurements

Fig. 6**b** summarizes the ankle angle at terminal stance (ATS) for each of the three animal groups measured every three weeks. The ATS of the PGC and PGC-NGF groups was significantly reduced in comparison to the Autograft group at weeks 3 (Autograft: 41.3 ± 2.5 ° vs PGC: 28 ± 1.8 ° vs PGC-NGF: 32.2 ± 2.6 °) and 6 (Autograft: 45.5 ± 2.3 ° vs PGC: 29.3 ± 1.5 ° vs PGC-NGF: 34.6 ± 2.9 °); however, gradual recovery was seen by weeks 9 and 12. It is noteworthy that at weeks 9 (Autograft: 51.4 ± 5 ° vs PGC: 36.9 ± 4.2 ° vs PGC-NGF: 44.6 ± 4.5 °) and 12 (Autograft: 48.3 ± 3.6 ° vs PGC: 37.7 ± 5.6 ° vs PGC-NGF: 45.1 ± 6.7 °), the PGC-NGF group showed improved ATS comparable to that of the PGC group without statistical significance. We had previously reported that the microgrooved surface patterned nerve graft conduit resulted in improved axonal regeneration within the conduit in comparison to a conduit without the guidance pattern, and its NGF releasing property may have improved nerve regenerative potential [27].

3.4.3. Evaluations of the isometric tetanic force and muscle weight ratio

The maximum isometric tetanic force measurements of TA muscles at week 6 showed significantly lower tetanic force in both the PGC group (21.4 ± 2.5%, $P < 0.001$) and the PGC-NGF group (37.1 ± 6.1%, $P < 0.05$) compared to the autograft group (63.9 ± 5.4%).

At week 12, however, the tetanic force of the PGC-NGF group (60.6 ± 6.6%) reached a level comparable to that of the Autograft group (68 ± 7.9%), as seen in Fig. 6**c**, whereas the PGC group's tetanic force (44.9 ± 6.2%) remained significantly lower than that in the Autograft group ($P < 0.05$). It is also noteworthy that at weeks 6 and 12, the isometric tetanic force of the PGC-NGF group was higher without statistical significance than that of the PGC group, which implies improved regenerative potential of the NGF.

For the TA muscle wet weight ratio, the PGC group (29.9 ± 2.4%) showed significantly lower muscle weight than the Autograft group (41.7 ± 4%) at week 6 ($P < 0.05$), which indicated more severe denervation muscle atrophy and less muscle recovery in this group (Fig. 6**d**). Lower muscle weight was also observed in the PGC-NGF group (31.4 ± 1.5%) at week 6. At week 12, the PGC group (45.3 ± 4.2%) and PGC-NGF group (52.7 ± 7.7%) regained and recovered muscle weight closer to that of the autograft group (68.3 ± 3.5%). The PGC-NGF group's recovery in muscle weight was comparably higher than that in the PGC group, without statistical sig-

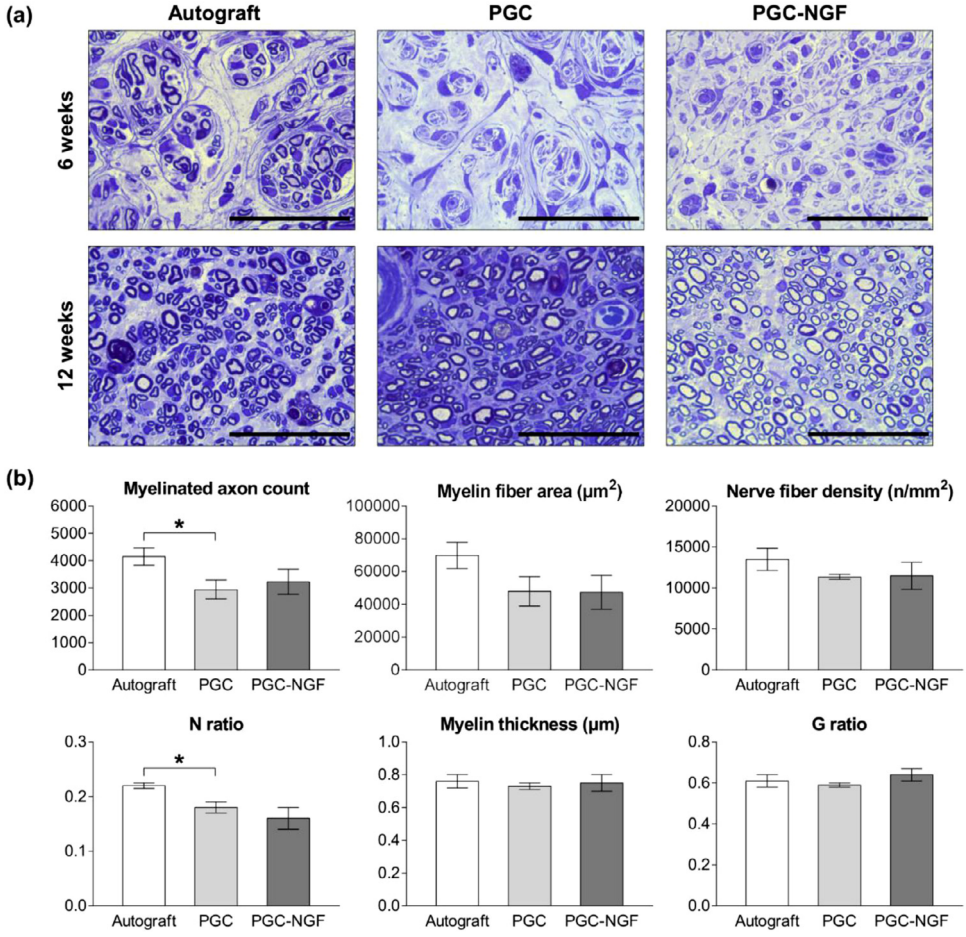

Fig. 7. *Histological and morphometrical analyses of the distal nerve in the in vivo rat sciatic nerve defect model.* (a) Toluidine blue staining of the distal nerve cross-section was performed for all experimental groups at 6 and 12 weeks after the operation. Scale bar = 50 μm. (b) Morphometrical analysis of the distal nerves at 12 weeks after the operation to assess the myelinated fibers. The number of myelinated axons, areas of the myelin fibers, density of the nerve fibers, N ratio, myelin thickness, and G ratio were measured and compared between the experimental groups ($n = 5$). ($^*P < 0.05$).

nificance. These results show that the NGF-loaded gelatin hydrogel used in this study may have promoted improved axonal regeneration over the gelatin hydrogel without NGF.

3.5. In vivo *rat study using PGC and PGC-NGF*

Nerve histology and morphometric analysis also revealed an improvement in axonal regeneration through NGC with NGF. Toluidine-blue-stained cross-sections were prepared at the distal level of each group at 6 and 12 weeks to reveal regenerated axons passing through each NGC after the operation. We utilized the nerve segment distal to the autograft and NGC for cross-section analyses to evaluate the final result of neural regeneration because it is the most appropriate location where Wallerian degeneration and axonal regeneration are evidently shown. Wallerian degeneration is an event that follows traumatic injury to PNS, nerve stumps that are located distal to lesion sites undergo the cellular changes that characterize Wallerian degeneration even though the area was not involved with direct trauma. Efficient cellular and molecular immune response of Wallerian degeneration, axonal sprouting, and its remyelination are critical to achieving good functional recovery [52]. As shown in Fig. 7**a**, axons and myelinated nerve fibers, as well as some endoneurial vessels, were observed in all experimental groups, implying adequate connection of the nerve through the NGC. Moreover, both at weeks 6 and 12, the density of regenerated axons was greater in the PGC-NGF group than in the PGC group.

Morphometric analyses of the nerve sections distal to the repair sites at 12 weeks were performed. The morphologies of the regenerated axons and surrounding myelin of the three groups were compared. Fig. 7**b** shows the results of the analyses including myelinated axon count, myelin fiber area, nerve fiber density, N ratio, myelin thickness, and G ratio measurements. A higher myelinated axon count was observed in the PGC-NGF group compared to the PGC group, but the difference was not statistically significant. With respect to the myelin fiber area, both the PGC group and the PGC-NGF group differed from the Autograft group in that the PGC and PGC-NGF group showed lower myelin fiber area in comparison to the Autograft group without statistical significance (Autograft: 69893 ± 15970 μm^2 vs PGC: 47952 ± 20229 μm^2 vs PGC-NGF: 47341 ± 20600 μm^2). Nerve fiber density was slightly higher in the Autograft group in comparison to the PGC and PGC-NGF group without statistical significance (Autograft: 13489 ± 2695 n mm^{-2} vs PGC: 11348 ± 688 n mm^{-2} vs PGC-NGF: 11486 ± 3305 n mm^{-2}). N ratio was comparably lower in the PGC and PGC-NGF group in comparison to the Autograft (Autograft: 0.2 ± 0.01 vs PGC: 0.2 ± 0.03 vs PGC-NGF: 0.2 ± 0.04). Myelin thickness and G ratio were similar in all three groups (Myelin thickness, Autograft: 0.8 ± 0.1 μm vs PGC: 0.7 ± 0.1 μm vs PGC-NGF: 0.8 ± 0.1 μm; G ratio, Autograft: 0.6 ± 0.1 vs PGC: 0.6 ± 0.03 vs PGC-NGF: 0.6 ± 0.1).

We have previously reported that the 3D printed intraluminal structure of a nerve graft conduit can improve the quality of ax-

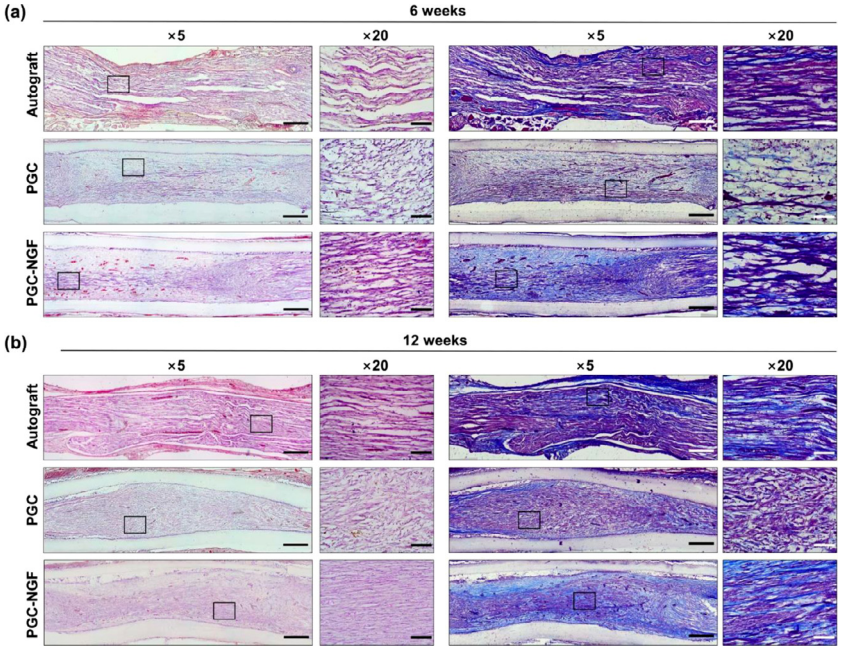

Fig. 8. *Hisotological analyses using hematoxylin-eosin (H&E) and Masson's trichrome (MT) staining*. Longitudinal sections of all experimental groups were stained at (a) 6 and (b) 12 weeks after the operation and analyzed under a light microscope. Scale bar = 500 μm at × 5 magnification, Scale bar = 100 μm at × 20 magnification.

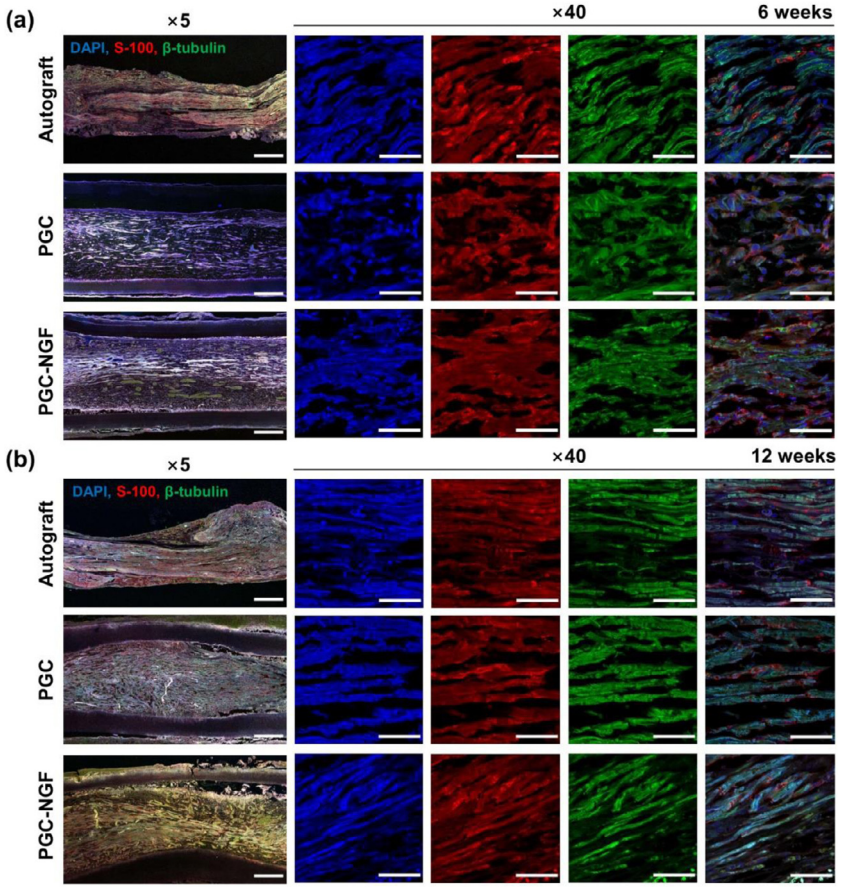

Fig. 9. *Immunohistochemical staining with DAPI (blue), S-100 (red), and β-tubulin (green)*. Longitudinal sections of all experimental groups were stained at (a) 6 and (b) 12 weeks after the operation and observed under the confocal laser scanning microscope (CLSM). Scale bar = 500 μm at × 5 magnification, Scale bar = 50 μm at × 40 magnification.

onal regeneration [27]. The intraluminal structure and aligned patterning of the collagen served as a guide for axonal growth in the conduit, as demonstrated by the histological sections. In this study, we showed that growth factors, such as NGF, along with the 3D printed intraluminal guiding structure, may promote further improvement in the axonal regeneration. Hence, we verified that the light-crosslinked gelatin hydrogel in NGCs with neuro-regenerative factors and bioactive molecules can optimize the nerve regeneration process and enhance the effective axonal sprouting in these 3D printed intraluminal structured conduits.

At 6 and 12 weeks after implantation, H&E, MT, and immunohistochemical staining were performed on the longitudinal sections of the regenerated nerves in the autograft, PGC, and PGC-NGF groups. Both PGC and PGC-NGF groups showed regenerative myelinated nerve fibers with alignment similar to that of the autograft group. Moreover, infiltration of the inflammatory cells around the regenerated nerves was not observed. Furthermore, H&E and MT staining demonstrated the formation and accumulation of collagen fibers (Fig. 8). We measured the percentage of collagen area from MT stained image, and there was no significant difference between the autograft (6 weeks: 40.9 $\pm$ 1.6%; 12 weeks: 42.5 $\pm$ 2.4%) and PGC-NGF group (6 weeks: 35.6 $\pm$ 4.5%; 12 weeks: 46.1 $\pm$ 2.7%) at both 6 and 12 weeks. The value of the PGC group increased from 6 weeks (20.2 $\pm$ 1.3%) to 12 weeks (32.2 $\pm$ 4%), but both values were lower than those of the PGC-NGF group **(Fig. S7a)**. Collagen consists of most of the connective tissue in the peripheral nerve and plays an important role in the growth of axons into the appropriate fascicles [53]. Therefore, the abundance of collagen is an indicator of successful axonal regeneration. We also performed immunohistochemical staining with S-100 (Schwann cells), β-tubulin (neurons), and DAPI (cell nuclei) across the longitudinal areas (Figs. 9 and **S6**). In both PGC and PGC-NGF groups, successful nerve regeneration occurred from the proximal stump to the distal stump *via* the implanted conduit. However, no significant differences were observed in the axonal myelination between the autograft and experimental groups, including PGC and PGC-NGF. The relative fluorescence intensity was also quantified from immunofluorescence (S-100 & β-tubulin) stained images. The result showed that there was no significant difference in the relative fluorescence intensity of S-100 and β-tubulin staining between the autograft group and experimental groups, including PGC and PGC-NGF **(Fig. S7b)**. This implies that 3D printed gelatin hydrogel successfully played the role of the inner guidance paths and provided effective assistance in nerve regeneration. It was also found that a higher density of aligned Schwann cells and neurons was observed in the PGC-NGF group than the PGC group, which suggests that the NGF released from the gelatin hydrogel supported the myelinated axons to regenerate nerves more effectively.

4. Conclusions

To enable effective nerve regeneration, bridge the gap in a transected nerve, and restore nervous system function, we developed an NGC formed by electrospun PLCL nanoporous membrane decorated with gelatin hydrogel-based inner guidance paths. In an *in vivo* rat study, we confirmed that the swellable 3D printed gelatin hydrogel paths developed microgrooved surface patterns and effectively assisted in the nerve regeneration process. In addition, the NGF-loaded gelatin hydrogel showed sustained release of bioactive NGF, resulting in enhanced nerve regeneration. This suggests that the light-crosslinked gelatin hydrogels can serve as delivery vehicles capable of embedding and releasing various bioactive molecules, including growth factors. Collectively, the PGC system designed in ths study are potential and valuable alternatives to autologous nerve grafts for the advanced treatment of neurological injuries.

Declaration of Competing Interest

The authors declare that they have no known competing financial interests or personal relationships that could have appeared to influence the work reported in this paper.

Acknowledgments

H.S. Lee, E.Y. Jeon, and J.J. Nam contributed equally to this work. This research was supported by the Translational Research Grant of the Korea University Medicine and Korea Institute of Science and Technology (K2107321 and 2E3115I) and grants of the Korea Regenerative Medical Technology Development Fund and the Nano•Material Technology Development Program (2021M3E5E5096098 and NRF2018M3A7B4071106) through the National Research Foundation of Korea funded by the Ministry of Science and ICT.

Supplementary materials

Supplementary material associated with this article can be found, in the online version, at doi:10.1016/j.actbio.2022.01.042.

References

[1] V. Carriel, M. Alaminos, I. Garzón, A. Campos, M. Cornelissen, Tissue engineering of the peripheral nervous system, Expert. Rev. Neurother. 14 (3) (2014) 301–318, doi:10.1586/14737175.2014.887444.
[2] R.M. Menorca, T.S. Fussell, J.C. Elfar, Peripheral nerve trauma: mechanisms of injury and recovery, Hand Clin. 29 (3) (2013) 317, doi:10.1016/j.hcl.2013.04.002.
[3] Y. Gao, Y.l. Wang, D. Kong, B. Qu, X.J. Su, H. Li, H.Y. Pi, Nerve autografts and tissue-engineered materials for the repair of peripheral nerve injuries: a 5-year bibliometric analysis, Neural Regen. Res. 10 (6) (2015) 1003, doi:10.4103/1673-5374.158369.
[4] A. Pabari, H. Lloyd-Hughes, A.M. Seifalian, A. Mosahebi, Nerve conduits for peripheral nerve surgery, Plast. Reconstr. Surg. 133 (6) (2014) 1420–1430, doi:10.1097/PRS.0000000000000226.
[5] A.M. Moore, R. Kasukurthi, C.K. Magill, H.F. Farhadi, G.H. Borschel, S.E. Mackinnon, Limitations of conduits in peripheral nerve repairs, Hand 4 (2) (2009) 180–186, doi:10.1007/s11552-008-9158-3.
[6] P. Ramburrun, P. Kumar, Y.E. Choonara, D. Bijukumar, L.C. du Toit, V. Pillay, A review of bioactive release from nerve conduits as a neurotherapeutic strategy for neuronal growth in peripheral nerve injury, Biomed. Res. Int. 2014 (2014), doi:10.1155/2014/132350.
[7] H. Jiang, Y. Qian, C. Fan, Y. Ouyang, Polymeric guide conduits for peripheral nerve tissue engineering, Front. Bioeng. Biotechnol. 8 (2020), doi:10.3389/fbioe.2020.582646.
[8] M. Sarker, S. Naghieh, A.D. McInnes, D.J. Schreyer, X. Chen, Strategic design and fabrication of nerve guidance conduits for peripheral nerve regeneration, Biotechnol. J. 13 (7) (2018) 1700635, doi:10.1002/biot.201700635.
[9] R. Boni, A. Ali, A. Shavandi, A.N. Clarkson, Current and novel polymeric biomaterials for neural tissue engineering, J. Biomed. Sci. 25 (1) (2018) 90, doi:10.1186/s12929-018-0491-8.
[10] D. Daranarong, R.T. Chan, N.S. Wanandy, R. Molloy, W. Punyodom, L. Foster, Electrospun polyhydroxybutyrate and poly (L-lactide-co-ε-caprolactone) composites as nanofibrous scaffolds, Biomed. Res. Int. (2014) 2014, doi:10.1155/2014/741408.
[11] R. Gaudin, C. Knipfer, A. Henningsen, R. Smeets, M. Heiland, T. Hadlock, Approaches to peripheral nerve repair: generations of biomaterial conduits yielding to replacing autologous nerve grafts in craniomaxillofacial surgery, Biomed. Res. Int. 2016 (2016), doi:10.1155/2016/3856262.
[12] S. Wang, L. Cai, Polymers for fabricating nerve conduits, Int. J. Polym. Sci. 2010 (2010), doi:10.1155/2010/138686.
[13] A.B. Bello, D. Kim, D. Kim, H. Park, S.H. Lee, Engineering and functionalization of gelatin biomaterials: from cell culture to medical applications, Tissue Eng. Part B Rev. 26 (2) (2020) 164–180, doi:10.1089/ten.teb.2019.0256.
[14] S.C. Wu, W.H. Chang, G.C. Dong, K.Y. Chen, Y.S. Chen, C.H. Yao, Cell adhesion and proliferation enhancement by gelatin nanofiber scaffolds, J. Bioact. Compat. Polym. 26 (6) (2011) 565–577, doi:10.1177/0883911511423563.
[15] I. Regas, F. Loisel, H. Haight, G. Menu, L. Obert, I. Pluvy, Rehabilitation, functionalized nerve conduits for peripheral nerve regeneration: a literature review, Hand Surg. Rehabilit. (2020), doi:10.1016/j.hansur.2020.05.007.
[16] P.A. Wieringa, A.R. Gonçalves de Pinho, S. Micera, R.J. van Wezel, L. Moroni, Biomimetic architectures for peripheral nerve repair: a review of biofabrication strategies, Adv. Healthc. Mater. 7 (8) (2018) 1701164, doi:10.1002/adhm.201701164.
[17] E.Y. Jeon, B.H. Hwang, Y.J. Yang, B.J. Kim, B.H. Choi, G.Y. Jung, H.J. Cha, Rapidly light-activated surgical protein glue inspired by mussel adhesion and insect structural crosslinking, Biomaterials 67 (2015) 11–19, doi:10.1016/j.biomaterials.2015.07.014.

[18] G.J. Clydesdale, G.W. Dandie, H.K Muller, Ultraviolet light induced injury: immunological and inflammatory effects, Immunol. Cell Biol. 79 (6) (2001) 547–568, doi:10.1046/j.1440-1711.2001.01047.x.
[19] S.I. Jeong, S.H. Kim, Y.H. Kim, Y. Jung, J.H. Kwon, B.S. Kim, Y.M. Lee, Manufacture of elastic biodegradable PLCL scaffolds for mechano-active vascular tissue engineering, J. Biomater. Sci. Polym. Ed. 15 (5) (2004) 645–660, doi:10.1163/156856204323046906.
[20] S.I. Jeong, B.S. Kim, S.W. Kang, J.H. Kwon, Y.M. Lee, S.H. Kim, Y.H. Kim, *In vivo* biocompatibilty and degradation behavior of elastic poly (l-lactide-co-ε-caprolactone) scaffolds, Biomaterials 25 (28) (2004) 5939–5946, doi:10.1016/j.biomaterials.2004.01.057.
[21] A. Wang, C. Xu, C. Zhang, Y. Gan, B. Wang, Experimental investigation of the properties of electrospun nanofibers for potential medical application, J. Nanomater. 2015 (2015), doi:10.1155/2015/418932.
[22] T.Y. Park, E.Y. Jeon, H.J. Kim, B.-H. Choi, H.J. Cha, Prolonged cell persistence with enhanced multipotency and rapid angiogenesis of hypoxia preconditioned stem cells encapsulated in marine-inspired adhesive and immiscible liquid micro-droplets, Acta Biomater. 86 (2019) 257–268, doi:10.1016/j.actbio.2019.01.007.
[23] ASTM D882-18Standard Test Method for Tensile Properties of Thin Plastic Sheeting, ASTM International, 2018, doi:10.1520/d0882-18.
[24] L. Cao, B. Cao, C. Lu, G. Wang, L. Yu, J. Ding, An injectable hydrogel formed by *in situ* cross-linking of glycol chitosan and multi-benzaldehyde functionalized PEG analogues for cartilage tissue engineering, J. Mater. Chem. B 3 (7) (2015) 1268–1280, doi:10.1039/c4tb01705f.
[25] M. Nadgorny, J. Collins, Z. Xiao, P.J. Scales, L.A. Connal, 3D-printing of dynamic self-healing cryogels with tuneable properties, Polym. Chem. 9 (13) (2018) 1684–1692, doi:10.1039/c7py01945a.
[26] J.Y. Lee, G. Giusti, H. Wang, P.F. Friedrich, A.T. Bishop, A.Y. Shin, Functional evaluation in the rat sciatic nerve defect model: a comparison of the sciatic functional index, ankle angles, and isometric tetanic force, Plast. Reconstr. Surg. 132 (5) (2013) 1173–1180, doi:10.1097/prs.0b013e3182a3bfeb.
[27] J. Yoo, J.H. Park, Y.W. Kwon, J.J. Chung, I.C. Choi, J.J. Nam, H.S. Lee, E.Y. Jeon, K. Lee, S.H. Kim, Augmented peripheral nerve regeneration through elastic nerve guidance conduits prepared using a porous PLCL membrane with a 3D printed collagen hydrogel, Biomater. Sci. 8 (22) (2020) 6261–6271, doi:10.1039/d0bm00847h.
[28] C. Helary, L. Ovtracht, B. Coulomb, G. Godeau, M.M. Giraud-Guille, Dense fibrillar collagen matrices: a model to study myofibroblast behaviour during wound healing, Biomaterials 27 (25) (2006) 4443–4452, doi:10.1016/j.biomaterials.2006.04.005.
[29] L. Chamberlain, I. Yannas, A. Arrizabalaga, H.P. Hsu, T. Norregaard, M. Spector, Early peripheral nerve healing in collagen and silicone tube implants: myofibroblasts and the cellular response, Biomaterials 19 (15) (1998) 1393–1403, doi:10.1016/s0142-9612(98)00018-0.
[30] C.B. Jenq, R.E. Coggeshall, Nerve regeneration through holey silicone tubes, Brain Res. 361 (1-2) (1985) 233–241, doi:10.1016/0006-8993(85)91294-6.
[31] C.B. Jenq, L.L. Jenq, R.E. Coggeshall, Nerve regeneration changes with filters of different pore size, Exp. Neurol. 97 (3) (1987) 662–671, doi:10.1016/0014-4886(87)90123-3.
[32] C.B. Jenq, R.E. Coggeshall, Permeable tubes increase the length of the gap that regenerating axons can span, Brain Res. 408 (1-2) (1987) 239–242, doi:10.1016/0006-8993(87)90379-9.
[33] E.B. Saltzman, J.C. Villa, S.B. Doty, J.H. Feinberg, S.K. Lee, S.W. Wolfe, A comparison between two collagen nerve conduits and nerve autograft: a rat model of motor nerve regeneration, J. Hand Surg. Am. 44 (8) (2019) 700 e1-700. e9, doi:10.1016/j.jhsa.2018.10.008.
[34] M. Ezra, J. Bushman, D. Shreiber, M. Schachner, J. Kohn, Porous and nonporous nerve conduits: the effects of a hydrogel luminal filler with and without a neurite-promoting moiety, Tissue Eng. Part A 22 (9-10) (2016) 818–826, doi:10.1089/ten.tea.2015.0354.
[35] X. Gu, F. Ding, Y. Yang, J. Liu, Construction of tissue engineered nerve grafts and their application in peripheral nerve regeneration, Prog. Neurobiol. 93 (2) (2011) 204–230, doi:10.1016/j.pneurobio.2010.11.002.
[36] M.P. Prabhakaran, J.R. Venugopal, S. Ramakrishna, Mesenchymal stem cell differentiation to neuronal cells on electrospun nanofibrous substrates for nerve tissue engineering, Biomaterials 30 (28) (2009) 4996–5003, doi:10.1016/j.biomaterials.2009.05.057.
[37] G.H. Borschel, K.F. Kia, W.M. Kuzon Jr, R.G. Dennis, Mechanical properties of acellular peripheral nerve, J. Surg. Res. 114 (2) (2003) 133–139, doi:10.1016/s0022-4804(03)00255-5.
[38] T. Dinis, R. Elia, G. Vidal, Q. Dermigny, C. Denoeud, D. Kaplan, C. Egles, F. Marin, 3D multi-channel bi-functionalized silk electrospun conduits for peripheral nerve regeneration, J. Mech. Behav. Biomed. Mater. 41 (2015) 43–55, doi:10.1016/j.jmbbm.2014.09.029.
[39] K. Stewart, P. Spedding, M. Otterburn, D. Lewis, Surface layer of wool. II. Dityrosine in wool, J. Appl. Polym. Sci. 66 (13) (1997) 2365–2376, doi:10.1002/(sici)1097-4628(19971226)66:13⟨2365::aid-app2⟩3.0.co;2-g.
[40] X. Liu, P.X. Ma, Phase separation, pore structure, and properties of nanofibrous gelatin scaffolds, Biomaterials 30 (25) (2009) 4094–4103, doi:10.1016/j.biomaterials.2009.04.024.
[41] E.O. Osidak, V.I. Kozhukhov, M.S. Osidak, S.P. Domogatsky, Collagen as bioink for bioprinting: a comprehensive review, Int. J. Bioprinting 6 (3) (2020), doi:10.18063/ijb.v6i3.270.
[42] R. Parenteau-Bareil, R. Gauvin, F. Berthod, Collagen-based biomaterials for tissue engineering applications, Materials 3 (3) (2010) 1863–1887, doi:10.3390/ma3031863.
[43] Q. Xing, K. Yates, C. Vogt, Z. Qian, M.C. Frost, F. Zhao, Increasing mechanical strength of gelatin hydrogels by divalent metal ion removal, Sci. Rep. 4 (2014) 4706, doi:10.1038/srep04706.
[44] J.H. George, D. Nagel, S. Waller, E. Hill, H.R. Parri, M.D. Coleman, Z. Cui, H. Ye, A closer look at neuron interaction with track-etched microporous membranes, Sci. Rep. 8 (1) (2018) 1–11, doi:10.1038/s41598-018-33710-6.
[45] G. Raivich, G. Kreutzberg, Nerve growth factor and regeneration of peripheral nervous system, Clin. Neurol. Neurosurg. 95 (1993) 84–88, doi:10.1016/0303-8467(93)90041-e.
[46] J. Kovalevich, D. Langford, Considerations for the use of SH-SY5Y neuroblastoma cells in neurobiology, Neuronal Cell Cult. (2013) 9–21 Springer, doi:10.1007/978-1-62703-640-5_2.
[47] Z. Yu, Y. Men, P. Dong, Schwann cells promote the capability of neural stem cells to differentiate into neurons and secret neurotrophic factors, Exp. Ther. Med. 13 (5) (2017) 2029–2035, doi:10.3892/etm.2017.4183.
[48] Q. Chai, Y. Jiao, X. Yu, Hydrogels for biomedical applications: their characteristics and the mechanisms behind them, Gels 3 (1) (2017) 6, doi:10.3390/gels3010006.
[49] C.D. Spicer, Hydrogel scaffolds for tissue engineering: the importance of polymer choice, Polym. Chem. 11 (2) (2020) 184–219, doi:10.1039/c9py01021a.
[50] J. Zhu, R.E. Marchant, Design properties of hydrogel tissue-engineering scaffolds, Expert Rev. Med. Devices 8 (5) (2011) 607–626, doi:10.1586/erd.11.27.
[51] Z. Wang, M. Lin, Q. Xie, H. Sun, Y. Huang, D. Zhang, Z. Yu, X. Bi, J. Chen, J. Wang, Electrospun silk fibroin/poly (lactide-co-ε-caprolactone) nanofibrous scaffolds for bone regeneration, Int. J. Nanomed. 11 (2016) 1483, doi:10.2147/ijn.s97445.
[52] S. Rotshenker, Wallerian degeneration: the innate-immune response to traumatic nerve injury, J. Neuroinflamm. 8 (1) (2011) 1–14, doi:10.1186/1742-2094-8-109.
[53] G. Koopmans, B. Hasse, N. Sinis, The role of collagen in peripheral nerve repair, Int. Rev. Neurobiol. 87 (2009) 363–379, doi:10.1016/s0074-7742(09)87019-0.